NANO LETTERS

Letter

pubs.acs.org/NanoLett

# Energy Transfer from Quantum Dots to Graphene and $MoS_2$: The Role of Absorption and Screening in Two-Dimensional Materials

Archana Raja,*[,†] Andrés Montoya−Castillo,[†] Johanna Zultak,[‡] Xiao-Xiao Zhang,[‡] Ziliang Ye,[‡] Cyrielle Roquelet,[‡] Daniel A. Chenet,[§] Arend M. van der Zande,[§] Pinshane Huang,[†] Steffen Jockusch,[†] James Hone,[§] David R. Reichman,[†] Louis E. Brus,[†] and Tony F. Heinz*[,∥,⊥]

[†]Department of Chemistry, [‡]Departments of Physics and Electrical Engineering, and [§]Department of Mechanical Engineering, Columbia University, New York, New York 10027, United States

[∥]Departments of Applied Physics and Photon Science, Stanford University, Stanford, California 94305, United States

[⊥]SLAC National Accelerator Laboratory, Menlo Park, California 94025, United States

Supporting Information

**ABSTRACT:** We report efficient nonradiative energy transfer (NRET) from core−shell, semiconducting quantum dots to adjacent two-dimensional sheets of graphene and $MoS_2$ of single- and few-layer thickness. We observe quenching of the photoluminescence (PL) from individual quantum dots and enhanced PL decay rates in time-resolved PL, corresponding to energy transfer rates of 1−10 $ns^{-1}$. Our measurements reveal contrasting trends in the NRET rate from the quantum dot to the van der Waals material as a function of thickness. The rate increases significantly with increasing layer thickness of graphene, but decreases with increasing thickness of $MoS_2$ layers. A classical electromagnetic theory accounts for both the trends and absolute rates observed for the NRET. The countervailing trends arise from the competition between screening and absorption of the electric field of the quantum dot dipole inside the acceptor layers. We extend our analysis to predict the type of NRET behavior for the near-field coupling of a chromophore to a range of semiconducting and metallic thin film materials.

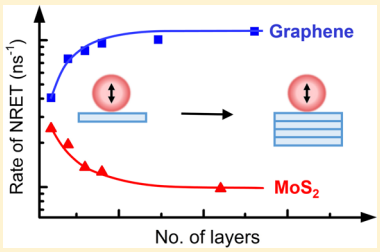


**KEYWORDS:** *Energy transfer, quantum dots, graphene, $MoS_2$, transition metal dichalcogenides, dielectric screening*

Metallic, semiconducting, and insulating nanostructures are available as building blocks for novel optoelectronic and photonic devices.[1−3] Near-field electromagnetic coupling of these materials plays an important role in the design of such devices. Colloidal semiconducting quantum dots (QD), which exhibit high quantum efficiencies and seamless tunability of bandgaps, are excellent absorbers and emitters of light. However, QD films have relatively poor carrier transport properties when compared to conventional semiconductors.[4] In contrast, graphite and the family of transition metal dichalcogenide (TMDC) crystals, which are composed of two-dimensional (2D) layers coupled by weak van der Waals' interactions, possess high mobilities.[5,6] Consequently, bringing these two classes of systems together for their respective strengths and understanding the interaction of photoexcited carriers in hybrid nanostructures is a burgeoning area of research.[7−11]

Nonradiative energy transfer (NRET) involves the transport of an excited electron−hole pair from an emitter or "donor" to an absorbing medium, or "acceptor". The coupling is mediated by near field interactions without the emission of photons and can be understood as the quenching of the donor dipole in the presence of a lossy medium.[12] The efficiency of NRET depends on a number of factors, including the distance between the donor and acceptor, the spectral overlap between the emission of the donor and absorption of the acceptor, the screening of the electric field of the donor dipole in the acceptor medium, and the dimensionality of the donor and acceptor.[13] NRET plays an important role in the transfer of energy through the photosynthetic network of plants,[14] solar cells,[15] and quantum-dot-based light-emitting diodes.[2] Because the efficiency of NRET is very sensitive to the separation between the donor and acceptor, it is used to measure distances in biological systems[16] and in nanoscale sensors with high specificity and low detection limits.[17,18] Engineering the spectral overlap between the donor and acceptor offers another way to control the NRET rate.[19] The complex environments in photosynthetic systems also require a greater understanding of the role of dielectric screening in tuning dipole−dipole coupling and the rate of energy transfer.[20,21]

With the emergence of two-dimensional materials like graphene and TMDC layers, there is a strong motivation, both for fundamental reasons and as underpinnings for potential applications, to extend our understanding of NRET to these novel systems. In particular, we wish to examine the prototypical case of energy transfer from a localized chromophore, such as zero-dimensional quantum dots, to these two-dimensional materials. Recently, there have been

**Received:** December 8, 2015
**Revised:** February 25, 2016
**Published:** March 1, 2016





DOI: 10.1021/acs.nanolett.5b05012
*Nano Lett.* 2016, 16, 2328−2333

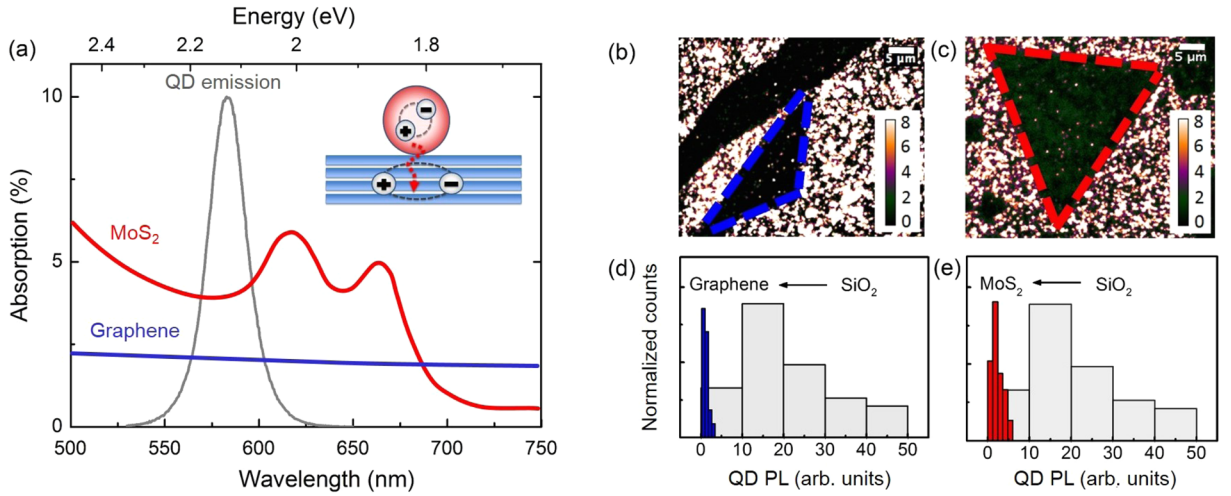


**Figure 1.** (a) Emission spectra of the QDs and the absorption spectra of monolayer graphene[23] and $MoS_2$.[24] Inset: Schematic representation of core−shell QD and the 2D layered material hybrid structure. (b,c) Wide-field photoluminescence images of QDs spin-cast on monolayer graphene (outlined by dashed blue lines) and $MoS_2$ (dashed red), respectively. The scale bars in the upper right corners are 5 $\mu$m in length. The contrast has been enhanced in the images to allow the quenched QDs on the monolayers to be discerned. (d,e) Statistics of the PL from hundreds of individual QDs for the two monolayers, revealing PL quenching of over 90% in both cases.

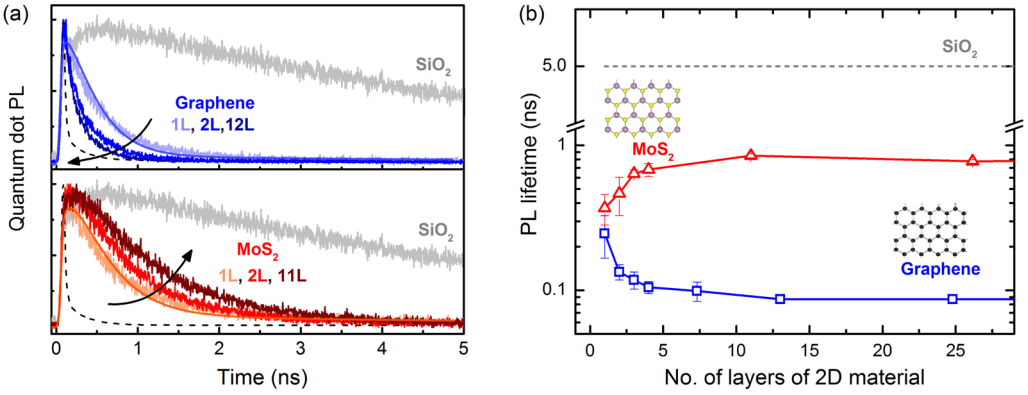


**Figure 2.** (a) TRPL traces on graphene layers are shown in the top panel and on $MoS_2$ in the bottom panel. Exemplary fits are overlaid on the data in solid blue and red lines. The gray trace corresponds to the $SiO_2$ substrate and the instrument response function is the dashed black line. (b) The QD lifetimes as a function of thickness of 2D layers are shown. Each data point corresponds to an average decay lifetime over multiple samples; the error bars represent the standard deviation of the measurements. The gray dashed line at 5 ns denotes the average lifetime of the dots on the $SiO_2$ substrate. The solid red and blue lines are guides to the eye.

independent reports of efficient NRET to graphene and $MoS_2$ based on different experimental techniques and theoretical models.[7,10,22,46] Chen et al.[7] reported an increasing rate of NRET with increasing thickness of the acceptor material, while Prins et al.[10] identified the opposite trend. Our goal is to examine and understand NRET to these 2D layers within a unified experimental and theoretical framework.

In this Letter, we report a direct experimental comparison of decay rates of quantum dot fluorescence when the chromophores are placed on graphene and $MoS_2$ layers of differing thickness. The measurements are performed using time-resolved photoluminescence (TRPL) and photoluminescence (PL) quenching of individual quantum dots on monolayer graphene and $MoS_2$. The increased PL decay rate observed for graphene and $MoS_2$ is attributed to NRET. Upon increasing the thickness of the acceptor material from monolayer to the bulk, the decay rate for the graphene layers increases, while that on $MoS_2$ decreases. For a given thickness, the rate is always found to be higher in the case of graphene. We show that a classical electromagnetic model with only the input of the materials' dielectric functions is sufficient to explain both the contrasting trends with the thickness of the 2D acceptor layer and the absolute rates within a factor of 2. The countervailing trends for the different material systems reflect differences in the relative importance of the additional layers on the absorption and screening of the local electric field.

**Experimental Methods.** CdSe/CdZnS core−shell quantum dots, provided by QD Vision Inc., were spin-cast from a dilute solution onto varying thicknesses of graphene and $MoS_2$ layers. The underlying substrate was a silicon wafer covered by a 285 nm $SiO_2$ film. The sample configuration is shown schematically in the inset of Figure 1a. The radius of the QDs was determined to be 5.4 nm through transmission electron microscopy; and the thicknesses of the 2D layers were established by a combination of Raman spectroscopy, atomic force microscopy, and optical contrast measurements.

For the time-resolved PL measurements, we excited the quantum dots with the frequency-doubled output of a modelocked Ti:sapphire laser providing 100 fs pulses of radiation at a wavelength of 405 nm at low pump fluences



DOI: 10.1021/acs.nanolett.5b05012
Nano Lett. 2016, 16, 2328−2333

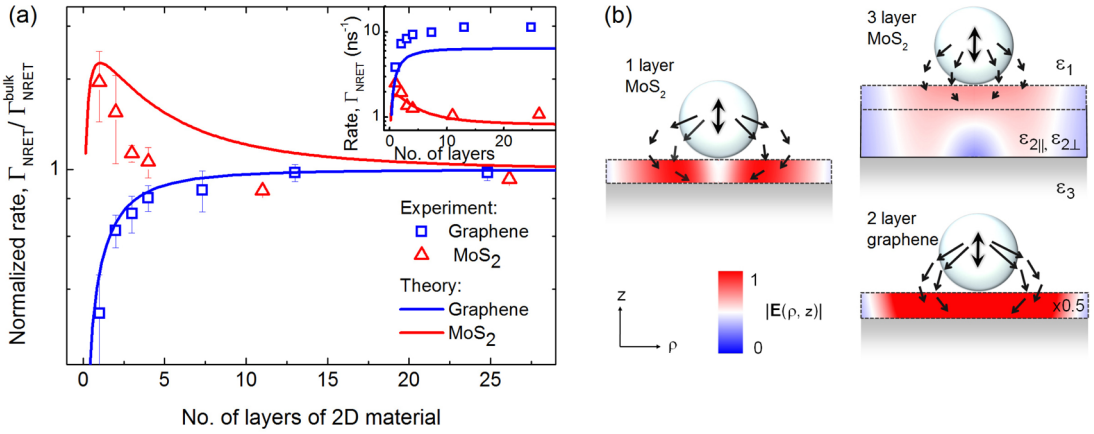


**Figure 3.** (a) Normalized rate of NRET from QDs to graphene and $MoS_2$ as a function of layer thickness. The rate of NRET on the respective bulk crystals are used for the normalization. Inset: Absolute rates of PL decay, presented as in the main figure. (b) Numerical simulations of the electric field of a QD dipole inside the acceptor layers. The black arrows represent the Poynting vectors, indicating the near-field transfer of energy from the QD to the underlying layer. The electric field has been reduced by a factor of 2 for the case of bilayer graphene.

(<1 $\mu J/cm^2$). We monitored the time evolution of the resulting PL through time correlated single photon counting using a fast avalanche photodiode. The instrument response function has a full width at half-maximum of 50 ps, which is appreciably smaller than our shortest measured lifetime. A similar detection scheme was employed to characterize the TRPL of isolated colloidal QDs using a suspension of QDs in toluene.

Steady-state diffraction-limited PL images of single QDs on monolayer graphene and $MoS_2$ were also measured. For this purpose, we made use of wide-field laser illumination of the sample. This measurement capability was applied to determine the PL quenching on the monolayers compared to the PL on the $SiO_2$ substrate. The PL from each QD was extracted by fitting the spatial profile of the emission to a 2D Gaussian form and integrating over the area of this diffraction-limited spot. Further information regarding the experimental techniques can be found in the Supporting Information (SI).

**Results and Discussion.** Figure 1a shows the spectral overlap between the optical absorption (at normal incidence) of the monolayer 2D materials and the optical emission spectra of the QDs. The two peaks in the $MoS_2$ absorption around 1.85 and 2 eV correspond to the "A" and "B" excitonic absorption features.[25] The wide-field images of single QD PL on monolayer graphene and $MoS_2$ are shown in panels b and c of Figure 1, respectively. Histograms of the PL intensity of individual QDs on graphene and $MoS_2$ are compared with that on $SiO_2$ in panels d and e, respectively, of Figure 1. In both cases, >90% of the PL is quenched on the 2D monolayers, as compared to the $SiO_2$ substrate. These results indicate the existence of efficient nonradiative decay channels for the photoexcited carriers in the QDs. The quenching also appears to be greater on graphene compared to $MoS_2$, despite its lower absorption at the emission energy of the QD.

Figure 2a displays the results of TRPL measurements at the QD emission energy. The population of photoexcited carriers decays relatively slowly in the absence of the 2D material. This is shown by the gray traces signifying QD emission on the $SiO_2$ substrate, which corresponds to a luminescence lifetime of 5 ns. When QDs are deposited on a monolayer of graphene (top panel, light blue trace) or of $MoS_2$ (bottom panel, light red trace), the PL lifetime drops by an order of magnitude. This finding is compatible with the observed PL quenching of individual QDs on the respective monolayer material. The lifetime data were fitted to a biexponential form (solid lines overlaid on the monolayer signals in Figure 2a) convoluted with the instrument response function (IRF, dotted black line in Figure 2a). The slower component of the biexponential decay is taken to have a fixed lifetime of 5 ns. Across all the measurements, the typical contribution of this component is on the order of a percent of the total signal. We attribute its presence to nonidealities in the QD film coverage, for example, to small regions with bilayer QD coverage.

For thicker layers of the 2D material, the observed PL lifetime of the QD decreases in the case of graphene until it approaches the bulk limit (blue traces in Figure 2a, b). The trend for the decay rates measured on graphene is consistent with the steady-state PL quenching experiments of Chen et al.[7] For $MoS_2$, however, the opposite trend is evident. The PL lifetime increases monotonically with layer thickness (red traces in Figure 2a, b). Monolayer $MoS_2$ yields more efficient NRET than bulk $MoS_2$ with the added layers of acceptor material effectively inhibiting energy transfer. This finding is in agreement with the observations of Prins et al.[10]

The total decay rate of QD excitation is given by the reciprocal of the measured PL emission time ($\Gamma = 1/\tau$). Assuming contributions to the decay rate other than NRET are unchanged as a function of layer thickness, $\Gamma_{NRET}$ can be obtained by subtracting the measured decay rate of the QDs on the bare $SiO_2$ substrate from the measured decay rate, $\Gamma$, on the material of interest. Figure 3a shows the resulting $\Gamma_{NRET}$ as a function of the number of layers of graphene and $MoS_2$, normalized by the rate of NRET on graphite and bulk $MoS_2$, respectively. In the following, we show that it is possible to understand and accurately model the opposing trends for $\Gamma_{NRET}$ using a simple electromagnetic treatment of energy transfer (solid lines in Figure 3a).

Within the electromagnetic picture of energy transfer, we model our experiment as a radiating dipole interacting with a lossy thin film. The key factors that contribute to $\Gamma_{NRET}$ are the dielectric function of the acceptor thin film, which for these anisotropic layers is represented by a (local) dielectric tensor ($\varepsilon = \varepsilon' + i\varepsilon''$), and the electric field ($\mathbf{E}$) distribution in the volume of the acceptor. In the classical approach, the rate of energy transfer from an oscillating dipole to an absorbing dielectric is then given by $\Gamma_{NRET} \propto \int_V d\nu\ \mathbf{E}^* \cdot \varepsilon'' \cdot \mathbf{E}$,[26] where $V$ is the volume of the lossy material. For the case of an isotropic


DOI: 10.1021/acs.nanolett.5b05012
Nano Lett. 2016, 16, 2328−2333

dielectric function, the expression can be simplified, such that $\Gamma_{NRET} \propto \varepsilon'' \int_V dv\ |\mathbf{E}|^2$. The rate is now proportional to the imaginary (or absorptive) component of the dielectric function, and the integrated intensity of the electric field set up by the radiating dipole in the acceptor layer.

The electric field within the acceptor layer depends on the complex dielectric function at the wavelength of the emitting dipole. For conditions relevant to our experiment, Figure 3b displays the magnitude of the electric field in the acceptor layers computed numerically.[27] Regardless of the value of $\varepsilon$, increasing the thickness of the thin film decreases the magnitude of the electric field in the top layer. This reflects screening of the electric field by the addition of polarizable material below the first layer. In Figure 3b, the electric field in the top layer of trilayer $MoS_2$ (dotted lines) is clearly weaker than in monolayer $MoS_2$. To gauge the effect of changing the dielectric function, while keeping the thickness of the material fixed, the electric field in monolayer $MoS_2$ is compared to the field in bilayer graphene (which has a similar thickness). The in-plane ($\varepsilon_{2\parallel} = 5.6 + 7i$) and out-of-plane ($\varepsilon_{2\perp} = 1.8 + 2i$) dielectric functions at the QD emission energy of 2.1 eV for graphene/graphite are taken from the literature[28,29] with corresponding values for $MoS_2$[24,30] of $18 + 9.3i$ and $16 + 2.2i$, respectively. Bilayer graphene exhibits a greater magnitude of the electric field in the thin film than a comparable thickness of $MoS_2$. Because the imaginary or absorptive components of the dielectric functions are similar in the case of graphene and $MoS_2$, the opposite trends of NRET with thickness in the two materials can be understood to arise from the differences in the total field strength inside the material. The electric field within a film of $MoS_2$ is screened so strongly with each added layer that it leads to a net decrease in the overall NRET with increasing thickness, despite the existence of additional decay channels for the thicker film. In the case of graphene, the screening of the electric field with each added layer, while still present, is weaker, and an increase in NRET with thickness is predicted.

With this qualitative picture in mind, we now calculate $\Gamma_{NRET}$ using the method introduced by Chance, Prock, and Silbey[26] and henceforth referred to as CPS theory. This approach offers an analytical alternative to the numerical solution described above. CPS theory treats the quantum mechanical transition dipole moment of the excitation in the QD coupled to excitations in underlying thin film as a radiating dipole near a lossy, anisotropic dielectric slab (as described schematically in Figure 3b).[31,32] The method yields compact integral expressions for the total and radiative components of the decay rate normalized by the decay rate of the radiating dipole in the absence of the lossy surface, $\Gamma/\Gamma_0$ and $\Gamma_{rad}/\Gamma_0$. The in-plane ($\varepsilon_{2\parallel}$) and out-of-plane ($\varepsilon_{2\perp}$) components of the dielectric functions for graphene and $MoS_2$ are from the taken from the literature, as above. When the material below the thin film provides larger screening than the material in which the QDs are embedded ($\varepsilon_1 < \varepsilon_3$, see Figure 3b), as in our experiment with the QDs in air and the thin film materials supported on an $SiO_2$ substrate, then $\Gamma_{NRET}/\Gamma_0$ does not simplify to the form used by previous authors.[10,33] It may, however, be obtained from $\Gamma_{NRET} = \Gamma - \Gamma_{rad}$. Expressions for the individual components of the rate are available in the literature[31] and are reproduced in the Supporting Information.

We find excellent agreement between the experimental results and the theoretical predictions of CPS theory, as indicated in Figure 3a for the relative rates and in the inset for the absolute rates. Relative rates ($\Gamma_{NRET}/\Gamma_{NRET}^{bulk}$) were calculated by normalizing the thin-film NRET rate by the rate on bulk film. In these calculations, we assume that the dielectric function of the thin films has no thickness dependence. While this is not strictly correct over the entire range of photon energies, we note the approximation holds well in the energy range of the QD emission at 2.1 eV.[24,34−36] Because CPS theory only yields the ratio $\Gamma_{NRET}/\Gamma_0$, the calculation of absolute rates requires an estimate of the QD decay rate in vacuum $\Gamma_0$, or, more practically, in a lossless solvent. Here, we employ the experimentally determined luminescence lifetime of the QDs in toluene (15 ns). More details are presented in the SI.

Despite being a classical macroscopic theory, the CPS approach has been shown to be equivalent to a perturbative quantum mechanical treatment, accurate to second order in the electronic coupling between the transition dipole moment of the radiating dipole and the excitations in the thin film.[26,37] For such a perturbative treatment to be valid, the coupling between the transition dipole moment of the QD and the excitations in the thin film material needs to be small compared to other energy scales of the system. A priori, one can use the localization radius, $\xi \sim 2$ nm, of the excitation in the QD and the distance between the center of the QD to the surface, $h \sim 5.4$ nm, as an estimate of the electronic coupling, $V \sim e^{-h/\xi} \ll 1$.[38]

We note that our discussion has neglected possible charge transfer processes that might contribute to the observed increase in the PL decay rate. This assumption is compatible with previous experimental work[39,40] on QD/carbon nanotube hybrid structures, which indicates that NRET is the dominant decay mechanism for photoexcited carriers in core−shell (type I) QDs. For efficient charge transfer, the bulky, aliphatic ligands passivating the surface of the QDs must be exchanged for shorter ones.[39,41] In the present work, along with the strong confinement of carriers in the core of the QD, surface passivation with long, insulating ligands (~1 nm long) greatly reduces the potential for charge transfer. Furthermore, the significant variation in the PL decay rate with the thickness of the 2D layers, as well as the prediction of these trends for NRET processes, indicate that charge transfer processes are not important under our experimental conditions.

The agreement of the classical electromagnetic theory with experiment highlights the versatility of the classical approach, which is applicable to both metallic and semiconducting thin films.[33] It thus provides a unified framework for understanding energy transfer for a wide array of single- to many-layer 2D materials. Of course, CPS theory is applicable only for the simple case where the excitation in the QD can be well approximated by a point dipole. The spherical core−shell structure of the QDs used in this experiment and the size of the dot being much smaller than the emission wavelength ensures that the dipole approximation is applicable.[42] Through numerical simulations, we have also confirmed that including the extended shell structure of the QD does not significantly alter the theoretical predictions. The additional screening of the QD dipole by the shell causes the rates to converge faster to the bulk limit compared to the point dipole approximation. The results can be found in Section 2.2 of the SI.

**Predictions for Other Systems.** Given the success of the CPS theory, we now examine in more detail what accounts for the two opposing trends in NRET rates with film thickness. First, we consider the factors that lead to maximum NRET to a thin film. We then provide a map for our experimental



DOI: 10.1021/acs.nanolett.5b05012
Nano Lett. 2016, 16, 2328−2333

conditions (emission energy of 2.1 eV and a separation of 5.4 nm) that identifies dielectric functions leading to a maximum in $\Gamma_{NRET}$ at finite thicknesses, the type of behavior exhibited by $MoS_2$. For simplicity, we restrict our analysis to a QD coupled to a thin film with an isotropic dielectric response.

We further assume the generic case of an absorbing material with $\varepsilon = 1 + \chi = 1 + |\chi|(1 + i)/\sqrt{2}$, that is, where the real and imaginary parts of the susceptibility are assumed to be equal. We then focus on the role of the magnitude of the susceptibility $|\chi|$, as shown in Figure 4a, in determining the behavior.

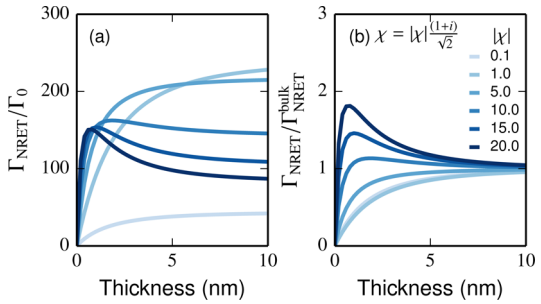


**Figure 4.** Variation of the NRET rate as a function of film thickness for different magnitudes of the susceptibility $\chi$ for $\varepsilon = 1 + |\chi|(1 + i)/\sqrt{2}$. The distance between the point dipole and the thin film is fixed at 5.4 nm. (a) The rate of NRET normalized by the decay rate of the dipole in vacuum. (b) The rate of NRET normalized by the value of the NRET rate in the bulk or large thickness limit.

For low values of $|\chi|$, where screening of the electric field is relatively weak, we see in Figure 4a that $\Gamma_{NRET}/\Gamma_0$ is characteristic of graphene-like behavior, that is, the maximum NRET is achieved in the limit of a thick film. As the total susceptibility is increased ($|\chi| = 10, 15, 20$), a suppression of the large-thickness rate is evident. The maximum $\Gamma_{NRET}/\Gamma_0$ occurs at finite thicknesses, as observed experimentally for the case of $MoS_2$. This trend is consistent with the intuitive argument introduced earlier: The greater the susceptibility, the greater the screening of the electric field within the thin film. For sufficiently strong screening, this effect outweighs the benefit of additional decay channels for the NRET process and leads to maximal decay for a film of finite thickness. In Figure 4b, we include the bulk-normalized rate of NRET, $\Gamma_{NRET}/\Gamma^{bulk}_{NRET}$. Although we lose the information on the absolute rates, it clearly identifies the cases that lead to a small-thickness peak in the NRET rate.

Finally, in Figure 5 we consider the influence of the complex dielectric function ($\varepsilon'$ and $\varepsilon''$) on the predicted trend with thickness for the same chromophore separation and photon energy as used to model our experiment. The goal is to identify the regions that lead to $MoS_2$-like behavior, that is, maxima in $\Gamma_{NRET}$ at finite thicknesses or $\Gamma^{max}_{NRET}/\Gamma^{bulk}_{NRET} > 1$. Note that when the absorptive component of the dielectric function ($\varepsilon''$) is zero, there is no NRET. We expand the dielectric functions considered to negative real components ($\varepsilon' < 0$) to model metals. We indicate a few common material systems based on their measured dielectric functions. The metals are identified in black and the nonmetals in white. The region enclosed within the dotted lines represents graphene-like behavior while the region outside displays $MoS_2$-like behavior. It is evident from Figure 5 that both the real and imaginary parts of the dielectric function play a role in determining the type of behavior. In the case of $MoS_2$ and graphene, they have similar absorptive

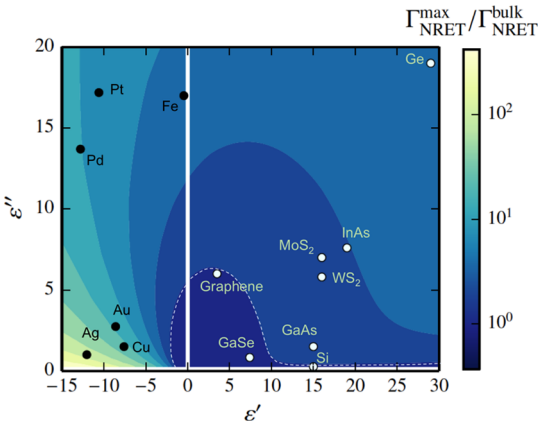


**Figure 5.** $\Gamma^{max}_{NRET}/\Gamma^{bulk}_{NRET}$ plotted as a function of the real and imaginary parts of the dielectric function. Rates corresponding to NRET from a point dipole to thin film with an isotropic dielectric function are calculated for a separation of 5.4 nm and emission photon energy of 2.1 eV. The dielectric functions are assumed to be constant as a function of film thickness. Some representative metals and semiconductors for applications in photovoltaics and optoelectronics are identified in the figure by their isotropically averaged dielectric constant at 2.1 eV.[24,43−45] The dotted lines enclose the region of dielectric space where the NRET rate increases monotonically with thickness. The larger excluded area corresponds to behavior where the peak NRET rate occurs for finite film thickness.

components ($\varepsilon''$) but the real part of $MoS_2$ is approximately three times that of graphene, leading to a stronger screening of the electric field. This results in the opposite trends observed for the thickness dependence of the NRET rates.

In conclusion, we have experimentally quantified the rate of NRET from QDs to graphene and $MoS_2$ through PL quenching and time-resolved PL for different thicknesses of the acceptor thin film. We have elucidated the opposite trends with thickness of graphene and $MoS_2$. The observations can be explained within a classical electromagnetic framework, where the differences in susceptibility lead to different balances between an increase in the available decay channels with increasing thickness and a decrease in the field strength from enhanced screening. The absolute rates of NRET are also successfully predicted by the theory.

## ■ ASSOCIATED CONTENT

### Supporting Information

The Supporting Information is available free of charge on the ACS Publications website at DOI: 10.1021/acs.nanolett.5b05012.

Detailed experimental methods are included, along with QD TRPL in toluene, transmission electron microscopy of the QDs, and Raman characterization of the graphene and $MoS_2$ layers. Details of the theory are also presented, including expressions for the radiative and nonradiative decay rates of a dipole near a thin-film and further discussion of the applicability of the model. (PDF)

## ■ AUTHOR INFORMATION

### Corresponding Authors

*E-mail: ar3125@columbia.edu.
*E-mail: tony.heinz@stanford.edu.



DOI: 10.1021/acs.nanolett.5b05012
Nano Lett. 2016, 16, 2328−2333

### Present Addresses

(J.Z.) Department of Micro- and Nanotechnology, Technical University of Denmark.

(A.M.v.d.Z.) Department of Mechanical Science and Engineering, University of Illinois at Urbana-Champaign, Urbana, IL 61801.

(P.H.) Department of Materials Science and Engineering, University of Illinois at Urbana-Champaign, Urbana, IL 61801.


### Author Contributions

A.M.−C. and J.Z. contributed equally to this work.

### Notes

The authors declare no competing financial interest.

## ■ ACKNOWLEDGMENTS

We thank Alexey Chernikov, Yinsheng Guo, Michael Steigerwald, and Ilan Jen-La Plante for many useful discussions. We also acknowledge Seth Coe-Sullivan and Jonathan Steckel of QD Vision, Inc. for providing the quantum dots used in this study and Marceau Hénot for development of codes for the analysis of wide-field PL images. This work was supported by the National Science Foundation MRSEC program through the Center for Precision Assembly of Superstratic and Superatomic Solids (Grant DMR-1420634), with additional funding for the single quantum dot imaging from the W. M. Keck Foundation, for the characterization of 2D materials from the Air Force Office of Scientific Research (Grant FA9550-14-1-0268) and for data analysis from the AMOS program, Chemical Sciences, Geosciences, and Biosciences Division, Basic Energy Sciences, Office of Science, US Department of Energy (Contract DE-AC02-76-SFO0515).

## ■ REFERENCES


(1) Geim, A. K.; Grigorieva, I. V. *Nature* **2013**, *499*, 419−25.

(2) Shirasaki, Y.; Supran, G. J.; Bawendi, M. G.; Bulović, V. *Nat. Photonics* **2012**, *7*, 13−23.

(3) Wang, C.; Takei, K.; Takahashi, T.; Javey, A. *Chem. Soc. Rev.* **2013**, *42*, 2592−2609.

(4) Konstantatos, G.; Sargent, E. H. *Nat. Nanotechnol.* **2010**, *5*, 391−400.

(5) Dean, C. R.; Young, A. F.; Meric, I.; Lee, C.; Wang, L.; Sorgenfrei, S.; Watanabe, K.; Taniguchi, T.; Kim, P.; Shepard, K. L.; Hone, J. *Nat. Nanotechnol.* **2010**, *5*, 722−726.

(6) Bao, W.; Cai, X.; Kim, D.; Sridhara, K.; Fuhrer, M. S. *Appl. Phys. Lett.* **2013**, *102*, 042104.

(7) Chen, Z.; Berciaud, S.; Nuckolls, C.; Heinz, T. F.; Brus, L. E. *ACS Nano* **2010**, *4*, 2964−2968.

(8) Konstantatos, G.; Badioli, M.; Gaudreau, L.; Osmond, J.; Bernechea, M.; de Arquer, F. P. G.; Gatti, F.; Koppens, F. H. L. *Nat. Nanotechnol.* **2012**, *7*, 363−368.

(9) Gaudreau, L.; Tielrooij, K. J.; Prawiroatmodjo, G. E. D. K.; Osmond, J.; García de Abajo, F. J.; Koppens, F. H. L. *Nano Lett.* **2013**, *13*, 2030−2035.

(10) Prins, F.; Goodman, A. J.; Tisdale, W. A. *Nano Lett.* **2014**, *14*, 6087−6091.

(11) Prasai, D.; Klots, A. R.; Newaz, A.; Niezgoda, J. S.; Orfield, N. J.; Escobar, C. A.; Wynn, A.; Efimov, A.; Jennings, G. K.; Rosenthal, S. J.; Bolotin, K. I. *Nano Lett.* **2015**, *15*, 4374−4380.

(12) Chance, R. R.; Prock, A.; Silbey, R. *J. Chem. Phys.* **1976**, *65*, 2527.

(13) Hernández-Martínez, P. L.; Govorov, A. O.; Demir, H. V. *J. Phys. Chem. C* **2014**, *118*, 4951−4958.

(14) Scholes, G. D.; Fleming, G. R.; Olaya-Castro, A.; van Grondelle, R. *Nat. Chem.* **2011**, *3*, 763−74.

(15) Hardin, B. E.; Snaith, H. J.; McGehee, M. D. *Nat. Photonics* **2012**, *6*, 162−169.

(16) Hillisch, A.; Lorenz, M.; Diekmann, S. *Curr. Opin. Struct. Biol.* **2001**, *11*, 201−207.

(17) Medintz, I. L.; Clapp, A. R.; Mattoussi, H.; Goldman, E. R.; Fisher, B.; Mauro, J. M. *Nat. Mater.* **2003**, *2*, 630−638.

(18) Chang, H.; Tang, L.; Wang, Y.; Jiang, J.; Li, J. *Anal. Chem.* **2010**, *82*, 2341−2346.

(19) Pons, T.; Medintz, I. L.; Sykora, M.; Mattoussi, H. *Phys. Rev. B: Condens. Matter Mater. Phys.* **2006**, *73*, 245302.

(20) Scholes, G. D.; Curutchet, C.; Mennucci, B.; Cammi, R.; Tomasi, J. *J. Phys. Chem. B* **2007**, *111*, 6978−6982.

(21) Curutchet, C.; Kongsted, J.; Muñoz Losa, A.; Hossein-Nejad, H.; Scholes, G. D.; Mennucci, B. *J. Am. Chem. Soc.* **2011**, *133*, 3078−3084.

(22) Swathi, R. S.; Sebastian, K. L. *J. Chem. Phys.* **2008**, *129*, 054703.

(23) Mak, K. F.; Ju, L.; Wang, F.; Heinz, T. F. *Solid State Commun.* **2012**, *152*, 1341−1349.

(24) Li, Y.; Chernikov, A.; Zhang, X.; Rigosi, A.; Hill, H. M.; van der Zande, A. M.; Chenet, D. A.; Shih, E.-M.; Hone, J.; Heinz, T. F. *Phys. Rev. B: Condens. Matter Mater. Phys.* **2014**, *90*, 205422.

(25) Mak, K. F.; Lee, C.; Hone, J.; Shan, J.; Heinz, T. F. *Phys. Rev. Lett.* **2010**, *105*, 136805.

(26) Chance, R. R.; Prock, A.; Silbey, R. *J. Chem. Phys.* **1975**, *62*, 2245.

(27) Comsol. COMSOL Multiphysics: Version 3.3. Comsol, 2006. http://www.comsol.com/.

(28) Weber, J. W.; Calado, V. E.; van de Sanden, M. C. M. *Appl. Phys. Lett.* **2010**, *97*, 091904.

(29) Jellison, G.; Hunn, J.; Lee, H. *Phys. Rev. B: Condens. Matter Mater. Phys.* **2007**, *76*, 085125.

(30) Daniels, J.; von Festenberg, C.; Raether, H.; Zeppenfeld, K. *Springer Tracts in Modern Physics*; Springer Tracts in Modern Physics; Springer-Verlag: Berlin/Heidelberg, 1970; Vol. *54*; pp 77−135.

(31) Novotny, L.; Hecht, B. *Principles of Nano-Optics*; Cambridge University Press: Cambridge, 2006.

(32) Chance, R. R.; Prock, A.; Silbey, R. *Adv. Chem. Phys.* **1978**, *37*, 1−64.

(33) Gordon, J. M.; Gartstein, Y. N. *J. Phys.: Condens. Matter* **2013**, *25*, 425302.

(34) Klintenberg, M.; Lebègue, S.; Ortiz, C.; Sanyal, B.; Fransson, J.; Eriksson, O. *J. Phys.: Condens. Matter* **2009**, *21*, 335502.

(35) Kumar, A.; Ahluwalia, P. *Phys. B* **2012**, *407*, 4627−4634.

(36) Ahuja, U.; Dashora, A.; Tiwari, H.; Kothari, D. C.; Venugopalan, K. *Comput. Mater. Sci.* **2014**, *92*, 451−456.

(37) Yeung, M. S.; Gustafson, T. K. *Phys. Rev. A: At., Mol., Opt. Phys.* **1996**, *54*, 5227−5242.

(38) May, V.; Kühn, O. *Charge and Energy Transfer Dynamics in Molecular Systems*; Wiley-VHC: New York, 2011.

(39) Peng, X.; Misewich, J. A.; Wong, S. S.; Sfeir, M. Y. *Nano Lett.* **2011**, *11*, 4562−4568.

(40) Shafran, E.; Mangum, B. D.; Gerton, J. M. *Nano Lett.* **2010**, *10*, 4049−4054.

(41) Kaniyankandy, S.; Rawalekar, S.; Ghosh, H. N. *J. Phys. Chem. C* **2012**, *116*, 16271−16275.

(42) Kristensen, P. T.; Mortensen, J. E.; Lodahl, P.; Stobbe, S. *Phys. Rev. B: Condens. Matter Mater. Phys.* **2013**, *88*, 205308.

(43) Aspnes, D. E.; Studna, A. A. *Phys. Rev. B: Condens. Matter Mater. Phys.* **1983**, *27*, 985−1009.

(44) Bianchi, D.; Emiliani, U.; Podini, P.; Paorici, C. *Phys. Status Solidi B* **1973**, *60*, 511−522.

(45) Rakić, A. D.; Djurišić, A. B.; Elazar, J. M.; Majewski, M. L. *Appl. Opt.* **1998**, *37*, 5271.

(46) Federspiel, F.; Froehlicher, G.; Nasilowski, M.; Pedetti, S.; Mahmood, A.; Doudin, B.; Park, S.; Lee, J.-O; Halley, D.; Dubertret, B.; Gilliot, P.; Berciaud, S. *Nano Lett.* **2015**, *15*, 1252−1258.




DOI: 10.1021/acs.nanolett.5b05012
*Nano Lett.* 2016, 16, 2328−2333